Electromagnetic form factors of octet baryons with the nonlocal chiral effective theory

Mingyang Yang[1,2] and P. Wang[1,3]

[1] *Institute of High Energy Physics, CAS, P. O. Box 918(4), Beijing 100049, China*

[2] *School of Physical Sciences, University of Chinese Academy of Sciences, Beijing 101408, China*

[3] *Theoretical Physics Center for Science Facilities, CAS, Beijing 100049, China*

The electromagnetic form factors of octet baryons are investigated with the nonlocal chiral effective theory. The nonlocal interaction generates both the regulator which makes the loop integral convergent and the Q^2 dependence of form factors at tree level. Both octet and decuplet intermediate states are included in the one loop calculation. The momentum dependence of baryon form factors are studied up to 1 GeV^2 with the same number of parameters as for the nucleon form factors. The obtained magnetic moments of all the baryon octets as well as the radii are in good agreement with the experimental data and/or lattice simulation.

I. INTRODUCTION

The study of electromagnetic form factors of hadrons is of crucial importance to understand their sub-structure. A lot of theoretical and experimental efforts have been made in this field. On the one hand, with the upgrade of the experimental facility, the parton distribution functions (PDFs) from the deep inelastic scattering as well as the form factors at relatively large momentum transfer from the elastic scattering can be extracted [1, 2]. On the other hand, many measurments on form factors have been carried out at very small momentum transfer to get the information of nucleon radii as accurate as possible [3, 4].

Theoretically, though QCD is the fundamental theory to describe strong interactions, it is difficult to study hadron physics using QCD directly. There are many phenomenological models, such as the cloudy bag model [5], the constituent quark model [6], the 1/Nc expansion approach [7], the Nambu-Jona-Lasino (NJL) model [8], the perturbative chiral quark model (PCQM) [9], the extended vector meson dominance model [10], the SU(3) chiral quark model [11], the quark-diquark model [12], etc. These model calculations are helpful to provide the physical scenario for the hadron structure.

Besides the phenomenological quark models, there are two systematic methods in hadron physics. One is the lattice simulation and the other is effective field theory (EFT) or chiral perturbation theory (ChPT). Historically, most formulations of ChPT are based on dimensional or infrared regularization. Though ChPT is a successful approach, for the nucleon electromagnetic form factors, it is only valid for $Q^2 < 0.1$ GeV^2 [13]. When vector mesons are included, the result is close to the experiments when Q^2 is less than 0.4 GeV^2 [14]. An alternative regularization method, namely finite-range-regularization (FRR) has been proposed. Inspired by quark models that account for the finite-size of the nucleon as the source of the pion cloud, effective field theory with FRR has been widely applied to extrapolate lattice data of vector meson mass, magnetic moments, magnetic form factors, strange form factors, charge radii, first moments of GPDs, nucleon spin, etc [15–24].

Recently, we proposed a nonlocal chiral effective Lagrangian which makes it possible to study the hadron properties at relatively large Q^2 [25, 26]. The nonlocal interaction generates both the regulator which makes the loop integral convergent and the Q^2 dependence of form factors at tree level. The obtained electromagnetic form factors and strange form factors of nucleon are very close to the experimental data [25, 26]. This nonlocal chiral effective theory was also applied to study the parton distribution functions and Sivers functions of sea quark in nucleon [27, 28]. In addition, the nonlocal behavior is further assumed to be a general property for all the interactions and an example of this assumption is the application to the lepton anomalous magnetic moments [29].

Since the nonlocal effective theory provides good descriptions to the nucleon form factors up to relatively large momentum transfer. In this paper, we will extend our study from nucleon to all the octet baryons. While the nucleon form factors are precisely determined experimentally, those of the other octet baryons are significantly more challenging to measure and as a result are poorly known from nature. Compared with the experiments, for the lattice gauge theory, it is not very difficult to extend the simulation of the nucleon form factors to the other octet form factors. Some lattice simulations on octet form factors have been reported [30–32]. Here, we will apply the nonlocal chiral effective theory to investigate the form factors of all the octet baryons. The paper is organized as follows. In section II, we will introduce the nonlocal chiral Lagrangian. The octet form factors are derived in section III. Numerical results are presented in section IV and finally, section V is a short summary.

II. CHIRAL EFFECTIVE LAGRANGIAN

The lowest order chiral Lagrangian for baryons, pseudo-scalar mesons and their interactions can be written as [25, 27, 33, 34],

$$\begin{aligned}\mathcal{L} &= i\,Tr\,\bar{B}\gamma_\mu \not{\mathscr{D}}^\mu B - m_B\,Tr\,\bar{B}B + \bar{T}^{abc}_\mu(i\gamma^{\mu\nu\alpha}D_\alpha\ -\ m_T\gamma^{\mu\nu})T^{abc}_\nu + \frac{f^2}{4}Tr\,\partial_\mu\Sigma\,\partial^\mu\Sigma^\dagger \\ &+ D\,Tr\,\bar{B}\gamma_\mu\gamma_5\,\{A_\mu, B\} + F\,Tr\,\bar{B}\gamma_\mu\gamma_5\,[A_\mu, B] + \frac{\mathcal{C}}{f}\epsilon^{abc}\bar{T}_{\mu,a}{}^{de}(g^{\mu\nu} + z\gamma_\mu\gamma_\nu)B_{ce}\partial_\nu\phi_{bd} + H.C,\end{aligned} \tag{1}$$

where D, F and $\mathcal{C}$ are the coupling constants. The chiral covariant derivative $\mathscr{D}_\mu$ is defined as $\mathscr{D}_\mu B = \partial_\mu B + [V_\mu, B]$. The pseudo-scalar meson octet couples to the baryon field via the vector and axial-vector combinations as

$$V_\mu = \frac{1}{2}(\zeta\partial_\mu\zeta^\dagger + \zeta^\dagger\partial_\mu\zeta) + \frac{1}{2}ie\mathscr{A}^\mu(\zeta^\dagger\,Q_c\,\zeta + \zeta\,Q_c\,\zeta^\dagger), \quad A_\mu = \frac{i}{2}(\zeta\partial_\mu\zeta^\dagger - \zeta^\dagger\partial_\mu\zeta) - \frac{1}{2}e\mathscr{A}^\mu(\zeta\,Q_c\,\zeta^\dagger - \zeta^\dagger\,Q_c\,\zeta), \tag{2}$$

where

$$\zeta^2 = \Sigma = e^{i2\phi/f}, \qquad f = 93\ \text{MeV}. \tag{3}$$

Q_c is the real charge matrix diag$(2/3, -1/3, -1/3)$. ϕ and B are the matrices of pseudo-scalar fields and octet baryons. $\mathscr{A}^\mu$ is the photon field. The covariant derivative D_μ in the decuplet sector is defined as $D_\nu T^{abc}_\mu = \partial_\nu T^{abc}_\mu + (\Gamma_\nu, T_\mu)^{abc}$, where Γ_ν is the chiral connection defined as $(X, T_\mu)^{abc} = (X)^a_d T^{dbc}_\mu + (X)^b_d T^{adc}_\mu + (X)^c_d T^{abd}_\mu$. $\gamma^{\mu\nu\alpha}$, $\gamma^{\mu\nu}$ are the antisymmetric matrices expressed as

$$\gamma^{\mu\nu} = \frac{1}{2}\left[\gamma^\mu, \gamma^\nu\right] \quad \text{and} \quad \gamma^{\mu\nu\rho} = \frac{1}{4}\left\{\left[\gamma^\mu, \gamma^\nu\right], \gamma^\rho\right\}. \tag{4}$$

The octet, decuplet and octet-decuplet transition operators for magnetic moment are needed in the one loop calculations. The baryon octet anomalous magnetic Lagrangian is written as

$$\mathcal{L}_{\text{oct}} = \frac{e}{4m_B}\Big(c_1\ \text{Tr}\left[\bar{B}\sigma^{\mu\nu}\left\{F^\dagger_{\mu\nu}, B\right\}\right] + c_2\ \text{Tr}\left[\bar{B}\sigma^{\mu\nu}\left[F^\dagger_{\mu\nu}, B\right]\right] + c_3\ \text{Tr}\left[\bar{B}\sigma^{\mu\nu}B\right]\ \text{Tr}\left[F^\dagger_{\mu\nu}\right]\Big), \tag{5}$$

where,

$$F^\dagger_{\mu\nu} = -\frac{1}{2}\left(\zeta^\dagger F_{\mu\nu}\,Q_c\,\zeta + \zeta F_{\mu\nu}\,Q_c\,\zeta^\dagger\right). \tag{6}$$

At the lowest order, the contribution of quark q with unit charge to the octet magnetic moments can be obtained by replacing the charge matrix Q_c with the corresponding diagonal quark matrices $\lambda_q = \text{diag}(\delta_{qu}, \delta_{qd}, \delta_{qs})$. Let's take the nucleon as an example. After expansion of the above equation, it is found that

$$\begin{aligned} &F_2^{p,u} = c_1 + c_2 + c_3, \quad &&F_2^{p,d} = c_3, \quad &&F_2^{p,s} = c_1 - c_2 + c_3, \\ &F_2^{n,u} = c_3, \quad &&F_2^{n,d} = c_1 + c_2 + c_3, \quad &&F_2^{n,s} = c_1 - c_2 + c_3. \end{aligned} \tag{7}$$

Comparing with the results of the constituent quark model where

$$F_2^{p,s} = 0 \ \text{ and } \ F_2^{n,s} = 0, \tag{8}$$

we get

$$\mathrm{c}_3 = \mathrm{c}_2 - \mathrm{c}_1. \tag{9}$$

The decuplet anomalous magnetic moment operator is expressed as

$$\mathcal{L}_{\text{dec}} = -\frac{ieF_2^T}{4M_T}\bar{T}_{\mu,abc}\sigma_{\rho\lambda}F^{\rho\lambda}T^{\mu,abc}. \tag{10}$$

The transition magnetic operator is written as

$$\mathcal{L}_{\rm trans} = i\frac{e}{4m_B}\mu_T F_{\mu\nu}\Big(\epsilon^{ijk}Q_{c,il}\bar{B}_{jm}\gamma^\mu\gamma_5\, T^{\nu,klm} + \epsilon^{ijk}Q_{c,li}\bar{T}^{\mu,klm}\,\gamma^\nu\gamma_5\, B_{mj}\Big). \tag{11}$$

The anomalous magnetic moments of baryons can also also be expressed in terms of quark magnetic moments μ_q. For example, $\mu_p = \frac{4}{3}\mu_u - \frac{1}{3}\mu_d$, $\mu_n = \frac{4}{3}\mu_d - \frac{1}{3}\mu_u$, $\mu_{\Delta^{++}} = 3\mu_u$. Using the SU(3) symmetry, $\mu_u = -2\mu_d = -2\mu_s$, μ_T and F_2^T as well as μ_q can be written in terms of c_1 or c_2. For example, $\mu_u = \frac{2}{3}c_1$, $\mu_T = 4c_1$, $F_2^{\Delta^{++}} = \mu_{\Delta^{++}} - 2 = 2c_1 - 2$.

The gauge invariant nonlocal Lagrangian can be obtained using the method in [25, 26, 35]. For instance, the local interaction between hyperons and K^- meson can be written as

$$\mathcal{L}_K^{\rm local} = \frac{D+F}{\sqrt{2}f}\bar{\Xi}^0(x)\gamma^\mu\gamma_5\,\Sigma^+(x)(\partial_\mu + ie\,\mathscr{A}_\mu(x))K^-(x). \tag{12}$$

The corresponding nonlocal Lagrangian is expressed as

$$\begin{aligned}\mathcal{L}_K^{\rm nl} = \frac{D+F}{\sqrt{2}f}\bar{\Xi}^0(x)\gamma^\mu\gamma_5\Sigma^+(x)\left(\partial_{x,\mu} + ie\int {\rm d}a\mathscr{A}_\mu(x-a)F(a)\right)\\ \times F(x-y)\exp\left[ie\int_x^y {\rm d}z_\nu\int\, {\rm d}a\mathscr{A}^\nu(z-a)F(a)\right]K^-(y),\end{aligned} \tag{13}$$

where $F(x)$ is the correlation function. To guarantee gauge invariance, the gauge link is introduced in the above Lagrangian. With the correlation function, the regulator can be generated automatically.

The nonlocal electromagnetic interaction can also be obtained in the same procedure,. For example, the local interaction between Σ^+ and photon is written as

$$\mathcal{L}_{EM}^{\rm local} = -e\bar{\Sigma}^+(x)\gamma^\mu\Sigma^+(x)\mathscr{A}_\mu(x) + \frac{(c_1+3c_2)e}{12m_\Sigma}\bar{\Sigma}^+(x)\sigma^{\mu\nu}\Sigma(x)^+F_{\mu\nu}(x). \tag{14}$$

The corresponding nonlocal Lagrangian is expressed as

$$\mathcal{L}_{EM}^{\rm nl} = -e\int {\rm d}a\bar{\Sigma}^+(x)\gamma^\mu\Sigma(x)^+\mathscr{A}_\mu(x-a)F_1(a) + \frac{(c_1+3c_2)e}{12m_\Sigma}\int {\rm d}a\bar{\Sigma}^+(x)\sigma^{\mu\nu}\Sigma(x)^+F_{\mu\nu}(x-a)F_2(a), \tag{15}$$

where $F_1(a)$ and $F_2(a)$ are the correlation functions for the nonlocal electric and magnetic interactions.

The momentum dependence of the form factors at tree level can be easily obtained with the Fourier transformation of the correlation function. As in our previous work [25, 26], the correlation function is chosen such that the charge and magnetic form factors at tree level have the same momentum dependence as the baryon-meson vertex, i.e. $G_M^{B,{\rm tree}}(q) = \mu_B G_E^{\rm tree}(q) = \mu_B\tilde{F}(q)$, where $\tilde{F}(q)$ is the Fourier transformation of the correlation function $F(a)$. Therefore, the corresponding functions $\tilde{F}_1(q)$ and $\tilde{F}_2(q)$ of Σ^+, for example, are expressed as,

$$\tilde{F}_1^{\Sigma^+}(q) = \tilde{F}(q)\frac{12{m_\Sigma}^2 + (3+c_1+3c_2)Q^2}{3(4{m_\Sigma}^2+Q^2)}, \quad \tilde{F}_2^{\Sigma^+}(q) = \tilde{F}(q)\frac{4(c_1+3c_2){m_\Sigma}^2}{3(4m_\Sigma^2+Q^2)}, \tag{16}$$

where $Q^2 = -q^2$ is the momentum transfer. From Eq. (13), two kinds of couplings between hadrons and photons can be obtained. One is the normal coupling, expressed as

$$\mathcal{L}^{\rm norm} = ie\frac{D+F}{\sqrt{2}f}\bar{\Xi}^0(x)\gamma^\mu\gamma_5\Sigma^+(x)\int\, {\rm d}a\mathscr{A}_\mu(x-a)F(a)F(x-y)K^-(y). \tag{17}$$

This interaction is similar to the traditional local Lagrangian except for the correlation function. The other is the additional interaction obtained by the expansion of the gauge link, expressed as

$$\mathcal{L}^{\rm add} = ie\frac{D+F}{\sqrt{2}f}\bar{\Xi}^0(x)\gamma^\mu\gamma_5\Sigma^+(x)\partial_{x,\mu}\Big(F(x-y)\int_x^y {\rm d}z_\nu\int {\rm d}a\mathscr{A}^\nu(z-a)F(a)K^-(y)\Big). \tag{18}$$

The additional interaction guarantees the charge conservation.

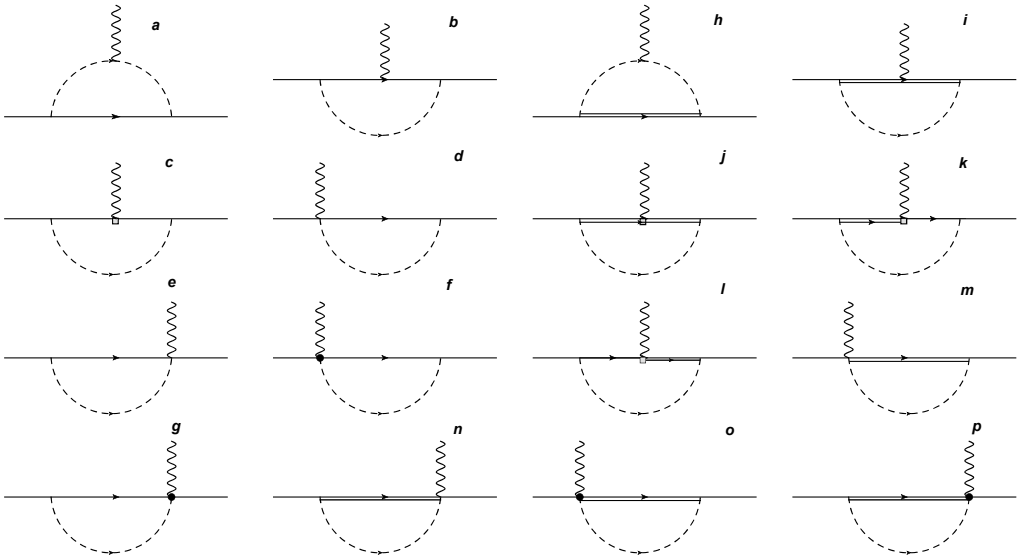

FIG. 1. One-loop Feynman diagrams for the octet electromagnetic form factors. The solid, double-solid, dashed and wave lines are for the octet baryons, decuplet baryons, pseudo-scalar mesons and photons, respectively. The rectangle and black dot represent magnetic and additional interacting vertex.

III. ELECTROMAGNETIC FORM-FACTORS

The Dirac and Pauli form factors of octet baryons are defined as

$$\langle B(p')|J_\mu|B(p)\rangle = \bar{u}(p')\left\{\gamma^\mu F_1^B(Q^2) + \frac{i\sigma^{\mu\nu}q_\nu}{2m_B}F_2^B(Q^2)\right\}u(p), \tag{19}$$

where $q = p' - p$. The electromagnetic form factors are defined as the combinations of the above form factors as

$$G_E^B(Q^2) = F_1^B(Q^2) - \frac{Q^2}{4m_B^2}F_2^B(Q^2), \quad G_M^B(Q^2) = F_1^B(Q^2) + F_2^B(Q^2). \tag{20}$$

With the electromagnetic form factors, the magnetic and electric (charge) radii can be obtained. The magnetic radii of octet baryons are defined as

$$\langle r_M^2\rangle_B = \frac{-6}{G_M^B(0)}\frac{\mathrm{d}G_M^B(Q^2)}{\mathrm{d}Q^2}|_{Q^2=0}. \tag{21}$$

The electric radii of charged and neutral baryons are defined as

$$\langle r_E^2\rangle_B = \frac{-6}{G_E^B(0)}\frac{\mathrm{d}G_E^B(Q^2)}{\mathrm{d}Q^2}|_{Q^2=0} \quad \text{and} \quad \langle r_E^2\rangle_B = -6\frac{\mathrm{d}G_E^B(Q^2)}{\mathrm{d}Q^2}|_{Q^2=0}, \tag{22}$$

respectively.

According to the Lagrangian, the one loop Feynman diagrams which contribute to the octet electromagnetic form factors are shown in Fig. 1. From the Lagrangian, we can get the matrix element of Eq. (19). Let's take the Σ hyperons as an example. In this section, we only show the expressions for the intermediate octet baryons. For the intermediate decuplet baryons, the expressions are similar but more complicated which are expressed in Appendix A.

The contributions of Fig. 1a are written as

$$\Gamma_a^\mu(\Sigma^-) = \frac{F^2}{f^2} I_a^{\Sigma\pi} + \frac{D^2}{3f^2} I_a^{\Lambda\pi} + \frac{(D-F)^2}{2f^2} I_a^{NK}, \tag{23}$$

$$\Gamma_a^\mu(\Sigma^0) = \frac{(D-F)^2}{4f^2} I_a^{NK} - \frac{(D+F)^2}{4f^2} I_a^{\Xi K}, \tag{24}$$

$$\Gamma_a^\mu(\Sigma^+) = -\frac{F^2}{f^2} I_a^{\Sigma\pi} - \frac{D^2}{3f^2} I_a^{\Lambda\pi} - \frac{(D+F)^2}{2f^2} I_a^{\Xi K}, \tag{25}$$

where the integral I_a^{BM} is expressed as

$$I_a^{BM} = \bar{u}(p')\tilde{F}(q) \int \frac{\mathrm{d}^4k}{(2\pi)^4} \frac{\tilde{F}(q+k)\tilde{F}(k)}{D_M(k+q)} \frac{-(2k+q)^\mu}{D_M(k)} (\not{k} + \not{q})\gamma_5 \frac{1}{\not{p} - \not{k} - m_B} \not{k}\gamma_5 u(p). \tag{26}$$

$D_M(k)$ is defined as

$$D_M(k) = k^2 - m_M^2 + i\epsilon. \tag{27}$$

m_B and m_M are the masses of the intermediate B baryon and M meson.

The contributions of Fig. 1b are expressed as

$$\begin{aligned}\Gamma_b^\mu(\Sigma^-) = {} & \frac{F\left(c_1 DQ^2 - F\left(\left(-2c_1+3c_2+3\right)Q^2 + 12m_\Sigma^2\right)\right)}{3f^2\left(4m_\Sigma^2+Q^2\right)} I_b^{\Sigma\pi} - \frac{c_1 DQ^2(D-3F)}{9f^2\left(4m_\Lambda^2+Q^2\right)} I_b^{\Lambda\pi} \\ & - \frac{c_1 Q^2(D-F)^2}{3f^2\left(4m_N^2+Q^2\right)} I_b^{NK} - \frac{(D+F)^2\left(\left(-c_1+3c_2+3\right)Q^2 + 12m_\Xi^2\right)}{6f^2\left(4m_\Xi^2+Q^2\right)} I_b^{\Xi K},\end{aligned} \tag{28}$$

$$\begin{aligned}\Gamma_b^\mu(\Sigma^0) = {} & \frac{2c_1F^2Q^2}{3f^2\left(4m_\Sigma^2+Q^2\right)} I_b^{\Sigma\pi} - \frac{c_1D^2Q^2}{9f^2\left(4m_\Lambda^2+Q^2\right)} I_b^{\Lambda\pi} \\ & + \frac{(D-F)^2\left(\left(-c_1+3c_2+3\right)Q^2 + 12m_N^2\right)}{12f^2\left(4m_N^2+Q^2\right)} I_b^{NK} - \frac{(D+F)^2\left(\left(c_1+3c_2+3\right)Q^2 + 12m_\Xi^2\right)}{12f^2\left(4m_\Xi^2+Q^2\right)} I_b^{\Xi K},\end{aligned} \tag{29}$$

$$\begin{aligned}\Gamma_b^\mu(\Sigma^+) = {} & \frac{F\left(c_1(-D)Q^2 + \left(2c_1+3c_2+3\right)FQ^2 + 12Fm_\Sigma^2\right)}{3f^2\left(4m_\Sigma^2+Q^2\right)} I_b^{\Sigma\pi} - \frac{c_1DQ^2(D+3F)}{9f^2\left(4m_\Lambda^2+Q^2\right)} I_b^{\Lambda\pi} \\ & + \frac{(D-F)^2\left(\left(c_1+3c_2+3\right)Q^2 + 12m_N^2\right)}{6f^2\left(4m_N^2+Q^2\right)} I_b^{NK} - \frac{c_1Q^2(D+F)^2}{3f^2\left(4m_\Xi^2+Q^2\right)} I_b^{\Xi K},\end{aligned} \tag{30}$$

where the integral I_b^{BM} is written as

$$I_b^{BM} = \bar{u}(p')\tilde{F}(q) \int \frac{\mathrm{d}^4k}{(2\pi)^4} \frac{\tilde{F}(k)^2}{D_M(k)} \not{k}\gamma_5 \frac{1}{\not{p}' - \not{k} - m_B} \gamma^\mu \frac{1}{\not{p} - \not{k} - m_B} \not{k}\gamma_5 u(p). \tag{31}$$

Fig. 1c is similar to Fig. 1b except for the magnetic interaction. The contributions of this diagram are written as

$$\Gamma_c^\mu(\Sigma^-) = \frac{2Fm_\Sigma\left(c_1(D+2F)-3c_2F\right)}{3f^2\left(4m_\Sigma^2+Q^2\right)}I_c^{\Sigma\pi} - \frac{2c_1D(D-3F)m_\Lambda}{9f^2\left(4m_\Lambda^2+Q^2\right)}I_c^{\Lambda\pi} \tag{32}$$
$$- \frac{2c_1(D-F)^2m_N}{3f^2\left(4m_N^2+Q^2\right)}I_c^{NK} + \frac{\left(c_1-3c_2\right)(D+F)^2m_\Xi}{3f^2\left(4m_\Xi^2+Q^2\right)}I_c^{\Xi K},$$

$$\Gamma_c^\mu(\Sigma^0) = \frac{4c_1F^2m_\Sigma}{3f^2\left(4m_\Sigma^2+Q^2\right)}I_c^{\Sigma\pi} - \frac{2c_1D^2m_\Lambda}{9f^2\left(4m_\Lambda^2+Q^2\right)}I_c^{\Lambda\pi} \tag{33}$$
$$- \frac{\left(c_1-3c_2\right)(D-F)^2m_N}{6f^2\left(4m_N^2+Q^2\right)}I_c^{NK} - \frac{\left(c_1+3c_2\right)(D+F)^2m_\Xi}{6f^2\left(4m_\Xi^2+Q^2\right)}I_c^{\Xi K},$$

$$\Gamma_c^\mu(\Sigma^+) = \frac{2Fm_\Sigma\left(c_1(-D)+2c_1F+3c_2F\right)}{3f^2\left(4m_\Sigma^2+Q^2\right)}I_c^{\Sigma\pi} - \frac{2c_1D(D+3F)m_\Lambda}{9f^2\left(4m_\Lambda^2+Q^2\right)}I_c^{\Lambda\pi} \tag{34}$$
$$+ \frac{\left(c_1+3c_2\right)(D-F)^2m_N}{3f^2\left(4m_N^2+Q^2\right)}I_c^{NK} - \frac{2c_1(D+F)^2m_\Xi}{3f^2\left(4m_\Xi^2+Q^2\right)}I_c^{\Xi K},$$

where I_c^{BM} is expressed as

$$I_c^{BM} = \bar{u}(p')\tilde{F}(q)\int\frac{\mathrm{d}^4k}{(2\pi)^4}\frac{\tilde{F}(k)^2}{D_M(k)}\not{k}\gamma_5\frac{1}{\not{p}'-\not{k}-m_B}i\sigma^{\mu\nu}q_\nu\frac{1}{\not{p}-\not{k}-m_B}\not{k}\gamma_5u(p). \tag{35}$$

Fig. 1d and 1e are the Kroll-Ruderman diagrams. The contributions of these two diagrams are written as

$$\Gamma_{d+e}^\mu(\Sigma^-) = \frac{F^2}{f^2}I_{d+e}^{\Sigma\pi} + \frac{D^2}{3f^2}I_{d+e}^{\Lambda\pi} + \frac{(D-F)^2}{2f^2}I_{d+e}^{NK}, \tag{36}$$

$$\Gamma_{d+e}^\mu(\Sigma^0) = \frac{(D-F)^2}{4f^2}I_{d+e}^{NK} - \frac{(D+F)^2}{4f^2}I_{d+e}^{\Xi K}, \tag{37}$$

$$\Gamma_{d+e}^\mu(\Sigma^+) = -\frac{F^2}{f^2}I_{d+e}^{\Sigma\pi} - \frac{D^2}{3f^2}I_{d+e}^{\Lambda\pi} - \frac{(D+F)^2}{2f^2}I_{d+e}^{\Xi K}, \tag{38}$$

where

$$I_{d+e}^{BM} = \bar{u}(p')\tilde{F}(q)\int\frac{\mathrm{d}^4k}{(2\pi)^4}\frac{\tilde{F}(k)^2}{D_M(k)}\left\{\not{k}\gamma_5\frac{1}{\not{p}'-\not{k}-m_B}\gamma^\mu\gamma_5 + \gamma^\mu\gamma_5\frac{1}{\not{p}-\not{k}-m_B}\not{k}\gamma_5\right\}u(p). \tag{39}$$

Fig. 1f and 1g are the additional diagrams which are generated from the expansion of the gauge link terms. The contributions of these two diagrams for intermediate octet hyperons are expressed as

$$\Gamma_{f+g}^\mu(\Sigma^-) = \frac{F^2}{f^2}I_{f+g}^{\Sigma\pi} + \frac{D^2}{3f^2}I_{f+g}^{\Lambda\pi} + \frac{(D-F)^2}{2f^2}I_{f+g}^{NK}, \tag{40}$$

$$\Gamma_{f+g}^\mu(\Sigma^0) = \frac{(D-F)^2}{4f^2}I_{f+g}^{NK} - \frac{(D+F)^2}{4f^2}I_{f+g}^{\Xi K}, \tag{41}$$

$$\Gamma_{f+g}^\mu(\Sigma^+) = -\frac{F^2}{f^2}I_{f+g}^{\Sigma\pi} - \frac{D^2}{3f^2}I_{f+g}^{\Lambda\pi} - \frac{(D+F)^2}{2f^2}I_{f+g}^{\Xi K}, \tag{42}$$

where

$$I_{f+g}^{BM} = \bar{u}(p')\tilde{F}(q)\int\frac{\mathrm{d}^4k}{(2\pi)^4}\frac{\tilde{F}(k)}{D_M(k)}\left\{\frac{(2k-q)^\mu}{2kq-q^2}[\tilde{F}(k-q)-\tilde{F}(k)]\not{k}\gamma_5\frac{1}{\not{p}'-\not{k}-m_B}(-\not{k}+\not{q})\gamma_5\right.$$
$$\left.+\frac{(2k+q)^\mu}{2kq+q^2}[\tilde{F}(k+q)-\tilde{F}(k)](\not{k}+\not{q})\gamma_5\frac{1}{\not{p}-\not{k}-m_B}\not{k}\gamma_5\right\}u(p). \tag{43}$$

Using Package-X [36] to simplify the loop integral, we can get the expressions for the Dirac and Pauli form factors. In the next section, we discuss the numerical results.

	Tree	Loop	Total	Lattice [37]	Lattice [31]	NJL [38]	PCQM [39]	Exp. [40]
μ_p	1.850	0.795	2.644 ± 0.159	2.4(2)	2.3(3)	2.78	2.735 ± 0.121	2.793
μ_n	-0.859	-1.126	-1.984 ± 0.216	$-1.59(17)$	$-1.45(17)$	-1.81	-1.956 ± 0.103	-1.913
μ_{Σ^+}	1.850	0.572	2.421 ± 0.147	2.27(16)	2.12(18)	2.62	2.537 ± 0.201	2.458 ± 0.010
μ_{Σ^0}	0.429	0.155	0.584 ± 0.077	–	–	–	0.838 ± 0.091	–
μ_{Σ^-}	-0.991	-0.262	-1.253 ± 0.008	$-0.88(8)$	$-0.85(10)$	-1.62	-0.861 ± 0.040	-1.160 ± 0.025
μ_Λ	-0.429	-0.165	-0.594 ± 0.057	–	–	–	-0.867 ± 0.074	-0.613 ± 0.004
μ_{Ξ^0}	-0.859	-0.521	-1.380 ± 0.169	$-1.32(4)$	$-1.07(7)$	-1.14	-1.690 ± 0.142	-1.250 ± 0.014
μ_{Ξ^-}	-0.991	0.266	-0.725 ± 0.077	$-0.71(3)$	$-0.57(5)$	-0.67	-0.840 ± 0.087	-0.651 ± 0.0025

TABLE I. The tree, loop and total contributions to the octet magnetic moments μ_B (in units of the nucleon magneton μ_N). The results from two lattice simulations, NJL and PCQM models as well as the experimental data are also listed.

IV. NUMERICAL RESULTS

The coupling constants between octet baryons and mesons are determined by the two parameters D and F. In the numerical calculations, the parameters are chosen as $D = 0.76$ and $F = 0.50$ ($g_A = D + F = 1.26$). The coupling constant $\mathcal{C}$ is chosen to be $2D$ which is the same as in Ref. [25, 41]. The off-shell parameter z is -1 [42].The covariant regulator is chosen to be dipole form [25–27]

$$\tilde{F}[k] = \frac{\Lambda^4}{(k^2 - m_j^2 - \Lambda^2)^2}, \tag{44}$$

where m_j is the meson mass for the baryon-meson interaction and it is zero for the hadron-photon interaction. It was found that when Λ was around 0.90 GeV, the obtained nucleon form factors are very close to the experimental data. Therefore, all the above parameters are predetermined. There are only two free parameters which are the low energy constants c_1 and c_2. In our previous calculation for the nucleon form factors, they are fitted by the experimental nucleon magnetic moments. Here, c_1 and c_2 are determined to be 1.288 and 0.420, which give the minimal standard variation χ^2 of the octet magnetic moments.

In Table I, the tree, loop and total contributions to the baryon magnetic moments obtained from the nonlocal chiral effective theory are listed. The error bar in our calculation is determined by varying Λ from 0.8 to 1.0 GeV. The results from two lattice simulations, NJL and PCQM models as well as the experimental data are also listed for comparison. From the table, one can see that all the magnetic moments of baryon octets are reasonably reproduced. The largest deviation from the experiments is for Ξs, where the calculated absolute values of magnetic moments of μ_{Ξ^0} and μ_{Ξ^-} are about 10% larger than experimental ones. For the other baryons, the deviation from the experiments is less than 5%. It is interesting that all the tree and loop contributions have the same signs except for Ξ^-, where the loop diagrams give the opposite contribution to the tree diagram. The data from lattice simulations are somewhat smaller which is partially due to the large pion mass and/or the neglecting of the disconnected contribution.

The magnetic form factors of charged octet baryons versus momentum transfer Q^2 are plotted in Fig. 2. The solid, dashed, dotted and dash-dotted lines are for proton, Σ^+, Σ^- and Ξ^-, respectively. It is clear the proton magnetic form factor is comparable with the experimental data up to 1 GeV^2. This is the advantage of the nonlocal chiral effective theory. The correlation function in the nonlocal Lagrangian makes the loop integral convergent. In the mean time, it provides the momentum dependence of the form factors at tree level, and as a result, the total form factors can be close to the experimental data up to relatively large Q^2. The other charged form factors have the similar momentum dependence as proton. Among them, Ξ^- decreases a little slower with the increasing Q^2. The magnetic radii are determined by the slops of the form factors at zero momentum transfer which will be discussed later.

The normalized magnetic form factors for the charge neutral baryons are plotted in Fig. 3. The solid, dashed, dotted and dash-dotted lines are for neutron, Σ^0, Λ and Ξ^0, respectively. The magnetic from factors of Σ^0, Λ and Ξ^0 are close to each other. The neutron magnetic form factor is a little smaller than the experimental data and it drops faster than the other three neutral baryons. All of the form factors have a dipole-like momentum dependence.

The tree, loop and total contributions to the magnetic radii of octet baryons are listed in Table II. The data from lattice simulation and phenomenological quark models are also listed for comparison. Though our central values for proton and neutron are a little larger than experiments, the results are still reasonable. The magnetic radii of octet baryons vary from 0.5 fm^2 to 0.9 fm^2, but show no simple dependence on baryon/quark mass. Ξ^- has the largest contribution at tree level. Because of the opposite contribution from the loop diagrams, its total radius is the smallest one. Amazing thing is though the values from different methods are quite different, the order of the values from the largest to smallest is the same. For example, Σ^- and Ξ^- have the largest and smallest magnetic radii, respectively.

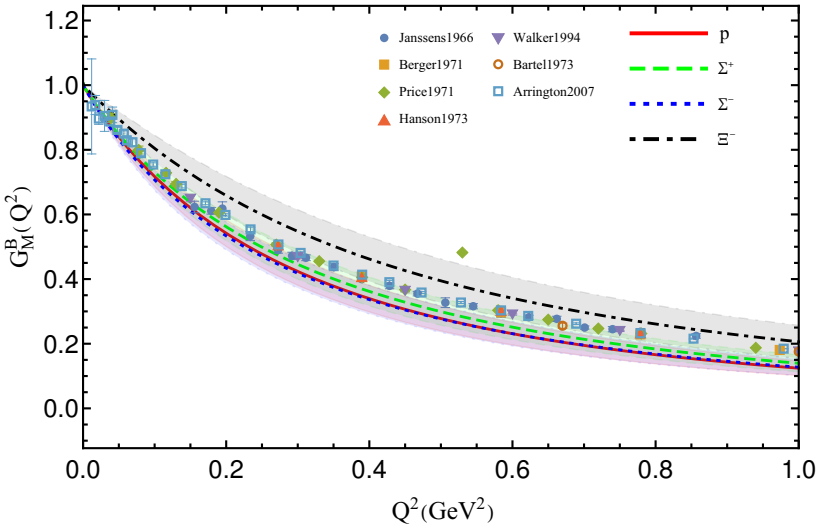

FIG. 2. The normalized magnetic form factors of charged octet baryons G_M^B/μ_B versus momentum transfer Q^2. The solid, dashed, dotted and dash-dotted lines are for proton, Σ^+, Σ^- and Ξ^-, respectively. The experimental form factor of proton is from Refs. [43–48].

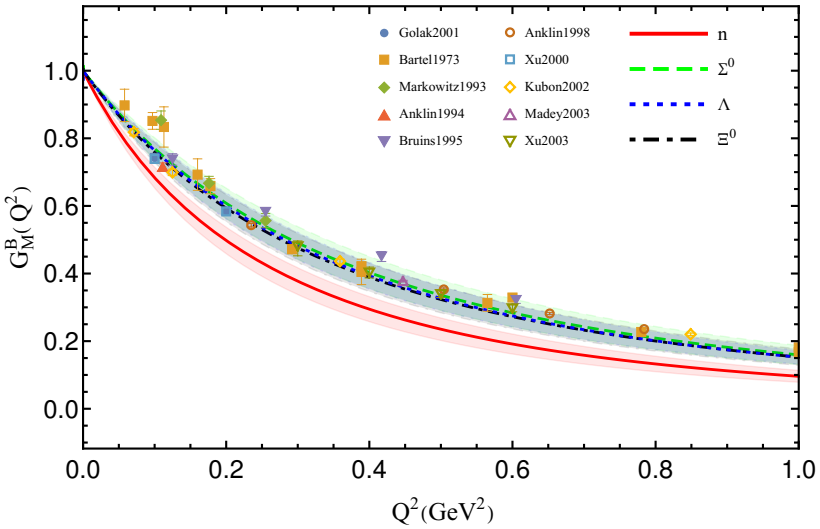

FIG. 3. The normalized magnetic form factors of neutral octet baryons G_M^B/μ_B versus momentum transfer Q^2. The solid, dashed, dotted and dash-dotted lines are for neutron, Σ^0, Λ and Ξ^0, respectively. The experimental form factor of neutron is from Refs. [46, 48–56].

The neutron magnetic radii is the second largest one. Our results also show the tree and loop contributions are strongly baryon dependent. The loop contribution to $\langle r_M^2\rangle_{\Sigma^0}$ is less than one half of the tree contribution. However, for neutron, the loop contribution is twice bigger than the tree contribution.

We now discuss the electric form factors. In Fig. 4, we plot the electric form factors of the charged baryons. Because of the additional interaction which makes the nonlocal Lagrangian locally gauge invariant, the electric form factors start from their charge at $Q^2 = 0$. The proton charge form factors is close to the experimental data. The absolute values of the electric form factors of charged baryons have the similar momentum dependence. This could be examined by the further experiments and/or accurate lattice simulation.

The electric form factors for the neutral baryons are plotted in Fig. 5. Again due to the charge conservation, the form factors start from 0 at zero momentum transfer. The calculated electric form factor of neutron is consistent with the experimental data. The form factors of the other neutral baryons are very small. There is no tree level

	Tree	Loop	Total	Lattice [30]	Lattice [31]	NJL [38]	PCQM [39]	Exp. [40]
$\langle r_M^2\rangle_p$	0.403	0.382	0.785 ± 0.132	0.470(48)	0.71(8)	0.76	0.909 ± 0.084	0.72 ± 0.04
$\langle r_M^2\rangle_n$	0.250	0.596	0.845 ± 0.148	0.478(50)	0.86(9)	0.83	0.922 ± 0.079	$0.746^{+0.016}_{-0.014}$
$\langle r_M^2\rangle_{\Sigma^+}$	0.441	0.324	0.765 ± 0.131	0.466(42)	0.66(5)	0.77	0.885 ± 0.094	–
$\langle r_M^2\rangle_{\Sigma^0}$	0.424	0.194	0.618 ± 0.124	0.432(38)	–	–	0.851 ± 0.102	–
$\langle r_M^2\rangle_{\Sigma^-}$	0.456	0.445	0.901 ± 0.119	0.483(49)	1.05(9)	0.92	0.951 ± 0.083	–
$\langle r_M^2\rangle_{\Lambda}$	0.417	0.203	0.620 ± 0.126	0.347(24)	–	–	0.852 ± 0.103	–
$\langle r_M^2\rangle_{\Xi^0}$	0.359	0.298	0.657 ± 0.128	0.384(22)	0.53(5)	0.44	0.871 ± 0.099	–
$\langle r_M^2\rangle_{\Xi^-}$	0.789	−0.255	0.534 ± 0.135	0.336(18)	0.44(5)	0.26	0.840 ± 0.109	–

TABLE II. The tree, loop and total contributions to the octet magnetic radii $\langle r_M^2\rangle_B$ (in units of fm^2). The results from two lattice simulations, NJL and PCQM models as well as the experimental data are also listed.

contribution to the electric form factors of neutral baryons and all the contributions are from the loop diagrams. Among them, neutron has the largest contribution from π-loop diagrams. The corresponding π-loop diagrams for the other neutral baryons are fairy small due to the small coupling constants.

The charge radii of octet baryons are listed in Table III. Our results are comparable with the experimental data in PDG for nucleon and Σ^-. A small proton charge radius $\langle r_E\rangle_p = 0.831 \pm 0.007 \pm 0.012$, i.e. $\langle r_E^2\rangle_p = 0.691 \pm 0.032$ was reported recently [3] which is also close to our value $\langle r_E^2\rangle_p = 0.729 \pm 0.112$. For the neutral baryons, the loop contribution is very small except neutron. For the charged baryons, the tree level contributions are the same which are also dominant for all of them. The loop contribution has the same order of magnitude except for Ξ^-, where the loop contribution is small. Different from the magnetic radii, the total charge radii vary around 0.6 and 0.7 fm^2 for the charged baryons.

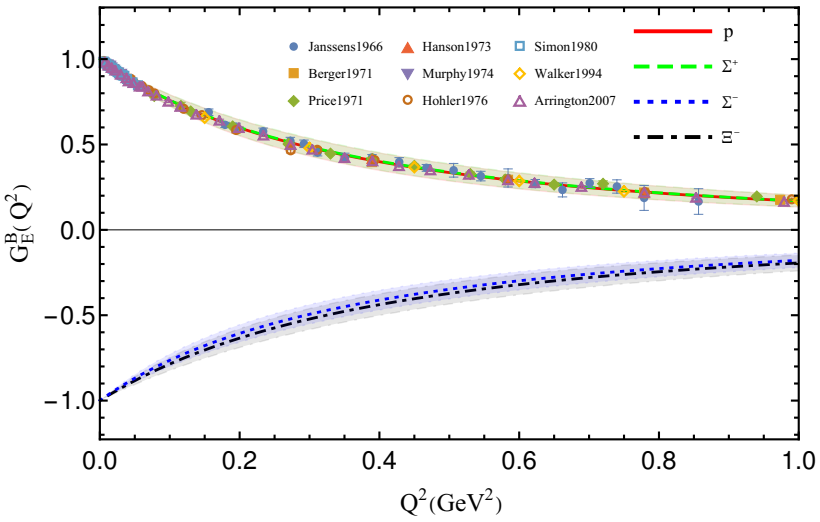

FIG. 4. Same as Fig. 2 but for electric form factors, The experimental form factor of proton is from Refs. [43–45, 47, 57–60].

V. SUMMARY

We applied the nonlocal chiral effective theory to study the electromagnetic form factors of octet baryons. The correlation function in the Lagrangian makes the loop integral convergent. It also provides the momentum dependence of the form factors at tree level. The additional interaction generated from the expansion of the gauge link guarantees the Lagrangian is locally gauge invariant. This nonlocal Lagrangian makes it possible to study the physical quantities at relatively large momentum transfer in the framework of chiral effective theory. In the numerical calculation, all the parameters are predetermined except the two low energy constants c_1 an c_2. They are fitted to give the minimum of the standard deviation. When extending the previous study of form factors of nucleon to all the baryon octets, we do not add any new parameter. The magnetic moments are well reproduced. The deviation from the experiments is less than 5% except Ξ^0 and Ξ^-, where the deviation is about 10%. For the radii, most experiments focus on the

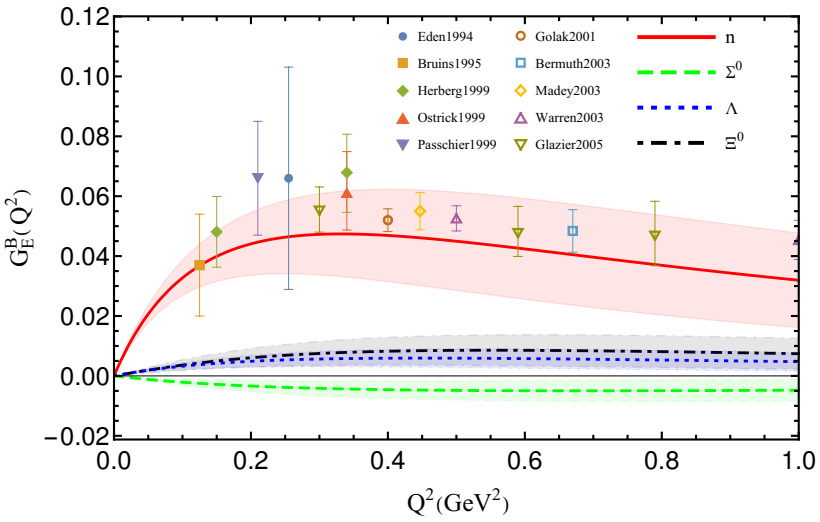

FIG. 5. Same as Fig. 3 but for electric form factors, The experimental form factor of neutron is from Refs. [49, 51, 55, 61–67].

	Tree	Loop	Total	Lattice [24]	Lattice [32]	NJL [38]	PCQM [39]	Exp. [40]
$\langle r_E^2\rangle_p$	0.577	0.152	0.729 ± 0.112	0.685(66)	0.76(10)	0.76	0.767 ± 0.113	0.7071 ± 0.0007
$\langle r_E^2\rangle_n$	0	−0.146	-0.146 ± 0.018	−0.158(33)	–	−0.14	-0.014 ± 0.001	-0.1161 ± 0.0022
$\langle r_E^2\rangle_{\Sigma^+}$	0.577	0.142	0.719 ± 0.116	0.749(72)	0.61(8)	0.92	0.781 ± 0.108	–
$\langle r_E^2\rangle_{\Sigma^0}$	0	0.010	0.010 ± 0.004	–	–	–	0	–
$\langle r_E^2\rangle_{\Sigma^-}$	0.577	0.123	0.700 ± 0.124	0.657(58)	0.45(3)	0.74	0.781 ± 0.063	0.61 ± 0.16
$\langle r_E^2\rangle_{\Lambda}$	0	−0.015	-0.015 ± 0.004	0.010(9)	–	–	0	–
$\langle r_E^2\rangle_{\Xi^0}$	0	−0.015	-0.015 ± 0.007	0.082(29)	–	0.24	0.014 ± 0.008	–
$\langle r_E^2\rangle_{\Xi^-}$	0.577	0.025	0.601 ± 0.127	0.502(47)	0.37(2)	0.58	0.767 ± 0.113	–

TABLE III. The tree, loop and total contributions to the octet charge radii $\langle r_E^2\rangle_B$ (in units of fm^2). The results from two lattice simulations, NJL and PCQM models as well as the experimental data are also listed.

nucleon and there is few data for the other baryons. Our results on magnetic and charge radii are comparable with the current experimental data. The calculated nucleon form factors are close to the experiments up to $Q^2 = 1$ GeV^2. For the other octet baryons, since the method is the same, we expect this nonlocal Lagrangian can also give good descriptions. The difference between our results and those of other theoretical methods could be examined by future experiments and more accurate lattice simulations.

ACKNOWLEDGMENTS

This work is supported by the National Natural Sciences Foundations of China under the grant No. 11975241, the Sino-German CRC 110 “Symmetries and the Emergence of Structure in QCD” project by NSFC under the grant No.11621131001.

Appendix A: Decuplet Expressions

In this section, we show the expressions of one loop integrals for decuplet intermediate states. The contribution for Fig. 1h can be written as

$$\Gamma_h^\mu(\Sigma^-) = \frac{\mathcal{C}^2}{12f^2} I_h^{\Sigma^*\pi} + \frac{\mathcal{C}^2}{6f^2} I_h^{\Delta K}, \tag{A1}$$

$$\Gamma_h^\mu(\Sigma^0) = -\frac{\mathcal{C}^2}{12f^2} I_h^{\Sigma^*\pi} + \frac{\mathcal{C}^2}{3f^2} I_h^{\Delta K}, \tag{A2}$$

$$\Gamma_h^\mu(\Sigma^+) = -\frac{\mathcal{C}^2}{12f^2} I_h^{\Sigma^*\pi} - \frac{\mathcal{C}^2}{6f^2} I_h^{\Xi^*\pi} + \frac{\mathcal{C}^2}{2f^2} I_h^{\Delta K}, \tag{A3}$$

where the integral I_h^{TM} is expressed as

$$I_h^{TM} = \bar{u}(p')\,\tilde{F}(q) \int \frac{\mathrm{d}^4k}{(2\pi)^4} \frac{\tilde{F}(q+k)\tilde{F}(k)}{D_M(k)} \frac{2(k+q)^\mu}{D_M(q+k)} \tag{A4}$$

$$\times((k+q)^\sigma + z(\not{k}+\not{q})\gamma^\sigma) \frac{1}{\not{p}-\not{k}-m_T} S_{\sigma\rho}(p-k)(-k^\rho - z\gamma^\rho \not{k})u(p). \tag{A5}$$

m_T is the mass of the decuplet intermediate state and $S_{\sigma\rho}(p)$ is expressed as

$$S_{\sigma\rho}(p) = -g_{\sigma\rho} + \frac{\gamma_\sigma\gamma_\rho}{3} + \frac{p_\sigma p_\rho}{3{m_T}^2} + \frac{\gamma_\sigma p_\rho - \gamma_\rho p_\sigma}{3m_T}. \tag{A6}$$

The contribution for Fig. 1i is written as

$$\Gamma_i^\mu(\Sigma^-) = -\frac{\mathcal{C}^2\left((c_1+3c_2+3)\,Q^2+12m_{\Sigma*}^2\right)}{36f^2\left(4m_{\Sigma*}^2+Q^2\right)} I_i^{\Sigma^*\pi} - \frac{\mathcal{C}^2\left((c_1+3c_2+3)\,Q^2+12m_{\Delta}^2\right)}{6f^2\left(4m_{\Delta}^2+Q^2\right)} I_i^{\Delta K} \tag{A7}$$

$$-\frac{\mathcal{C}^2\left((c_1+3c_2+3)\,Q^2+12m_{\Xi*}^2\right)}{18f^2\left(4m_{\Xi*}^2+Q^2\right)} I_i^{\Xi^*K},$$

$$\Gamma_i^\mu(\Sigma^0) = \frac{\mathcal{C}^2\left((c_1+3c_2+3)\,Q^2+12m_{\Delta}^2\right)}{9f^2\left(4m_{\Delta}^2+Q^2\right)} I_i^{\Delta K} - \frac{\mathcal{C}^2\left((c_1+3c_2+3)\,Q^2+12m_{\Xi*}^2\right)}{36f^2\left(4m_{\Xi*}^2+Q^2\right)} I_i^{\Xi^*K}, \tag{A8}$$

$$\Gamma_i^\mu(\Sigma^+) = \frac{\mathcal{C}^2\left((c_1+3c_2+3)\,Q^2+12m_{\Sigma*}^2\right)}{36f^2\left(4m_{\Sigma*}^2+Q^2\right)} I_i^{\Sigma^*\pi} + \frac{7\mathcal{C}^2\left((c_1+3c_2+3)\,Q^2+12m_{\Delta}^2\right)}{18f^2\left(4m_{\Delta}^2+Q^2\right)} I_i^{\Delta K}, \tag{A9}$$

where the integral I_i^{TM} is written as

$$I_i^{TM} = \bar{u}(p')\,\tilde{F}(q) \int \frac{\mathrm{d}^4k}{(2\pi)^4} \frac{\tilde{F}(k)^2}{D_M(k)} (k^\sigma + z\not{k}\gamma^\sigma) \tag{A10}$$

$$\times \frac{1}{\not{p}'-\not{k}-m_T} S_{\sigma\alpha}(p'-k)\gamma^{\alpha\beta\mu} \frac{1}{\not{p}-\not{k}-m_T} S_{\beta\rho}(p-k)(k^\rho + z\gamma^\rho \not{k})u(p). \tag{A11}$$

The contribution for Fig. 1j is written as

$$\Gamma_j^\mu(\Sigma^-) = \frac{(c_1+3c_2)\,\mathcal{C}^2 m_{\Sigma*}}{18f^2\left(4m_{\Sigma*}^2+Q^2\right)} I_j^{\Sigma^*\pi} + \frac{(c_1+3c_2)\,\mathcal{C}^2 m_{\Delta}}{3f^2\left(4m_{\Delta}^2+Q^2\right)} I_j^{\Delta K} + \frac{(c_1+3c_2)\,\mathcal{C}^2 m_{\Xi*}}{9f^2\left(4m_{\Xi*}^2+Q^2\right)} I_j^{\Xi^*K}, \tag{A12}$$

$$\Gamma_j^\mu(\Sigma^0) = -\frac{2\,(c_1+3c_2)\,\mathcal{C}^2 m_{\Delta}}{9f^2\left(4m_{\Delta}^2+Q^2\right)} I_j^{\Delta K} + \frac{(c_1+3c_2)\,\mathcal{C}^2 m_{\Xi*}}{18f^2\left(4m_{\Xi*}^2+Q^2\right)} I_j^{\Xi^*K}, \tag{A13}$$

$$\Gamma_j^\mu(\Sigma^+) = -\frac{(c_1+3c_2)\,\mathcal{C}^2 m_{\Sigma*}}{18f^2\left(4m_{\Sigma*}^2+Q^2\right)} I_j^{\Sigma^*\pi} - \frac{7\,(c_1+3c_2)\,\mathcal{C}^2 m_{\Delta}}{9f^2\left(4m_{\Delta}^2+Q^2\right)} I_j^{\Delta K}, \tag{A14}$$

where the integral I_j^{TM} is expressed as

$$I_j^{TM} = \bar{u}(p')\,\tilde{F}(q)\int\frac{\mathrm{d}^4k}{(2\pi)^4}\,\frac{\tilde{F}(k)^2}{D_M(k)}(k^\sigma + z\not{k}\gamma^\sigma) \tag{A15}$$

$$\times\frac{1}{\not{p}' - \not{k} - m_T}S_{\sigma\nu}(p'-k)i\sigma^{\mu\lambda}q_\lambda\frac{1}{\not{p} - \not{k} - m_T}S^{\nu\rho}(p-k)(k_\rho + z\gamma_\rho\not{k})u(p). \tag{A16}$$

The contribution for the intermediate octet-decuplet transition diagrams Fig. 1 k & l is expressed as

$$\Gamma^\mu_{k+l}(\Sigma^-) = -\frac{c_1\mathcal{C}F}{12f^2m_\Sigma}I^{\Sigma^*\Sigma\pi}_{k+l} + \frac{c_1\mathcal{C}D}{12f^2m_\Lambda}I^{\Sigma^*\Lambda\pi}_{k+l} + \frac{c_1\mathcal{C}(D-F)}{6f^2m_N}I^{\Delta NK}_{k+l}, \tag{A17}$$

$$\Gamma^\mu_{k+l}(\Sigma^0) = -\frac{c_1\mathcal{C}F}{6f^2m_\Sigma}I^{\Sigma^*\Sigma\pi}_{k+l} - \frac{c_1\mathcal{C}(D+F)}{12f^2m_\Xi}I^{\Xi^*\Xi K}_{k+l}, \tag{A18}$$

$$\Gamma^\mu_{k+l}(\Sigma^+) = -\frac{c_1\mathcal{C}F}{4f^2m_\Sigma}I^{\Sigma^*\Sigma\pi}_{k+l} - \frac{c_1\mathcal{C}D}{12f^2m_\Lambda}I^{\Sigma^*\Lambda\pi}_{k+l} - \frac{c_1\mathcal{C}(D-F)}{6f^2m_N}I^{\Delta NK}_{k+l} - \frac{c_1\mathcal{C}(D+F)}{6f^2m_\Xi}I^{\Xi^*\Xi K}_{k+l}, \tag{A19}$$

where the integral I^{TBM}_{k+l} is written as,

$$\begin{aligned} I^{TBM}_{k+l} = \bar{u}(p')\tilde{F}(q)\int\frac{\mathrm{d}^4k}{(2\pi)^4}\,\frac{\tilde{F}(k)^2}{D_M(k)}\Big\{&\not{k}\gamma_5\frac{1}{\not{p}' - \not{k} - m_B}(-\not{q})\gamma_5\frac{1}{\not{p} - \not{k} - m_T}S^{\mu\rho}(p-k)(k_\rho + z\gamma_\rho\not{k}) \\ &+\not{k}\gamma_5\frac{1}{\not{p}' - \not{k} - m_B}\gamma^\mu\gamma_5 q_\nu\frac{1}{\not{p} - \not{k} - m_T}S^{\nu\rho}(p-k)(k_\rho + z\gamma_\rho\not{k}) \\ &+(k_\nu + z\not{k}\gamma_\nu)\frac{1}{\not{p}' - \not{k} - m_T}S^{\nu\rho}(p'-k)(-q_\rho)\gamma^\mu\gamma_5\frac{1}{\not{p} - \not{k} - m_B}\not{k}\gamma_5 \\ &+(k_\nu + z\not{k}\gamma_\nu)\frac{1}{\not{p}' - \not{k} - m_T}S^{\nu\mu}(p'-k)\not{q}\gamma_5\frac{1}{\not{p} - \not{k} - m_B}\not{k}\gamma_5\Big\}u(p). \end{aligned} \tag{A20}$$

The contribution for the Kroll-Ruderman diagrams Fig. 1 m & n is written as

$$\Gamma^\mu_{m+n}(\Sigma^-) = \frac{\mathcal{C}^2}{12f^2}I^{\Sigma^*\pi}_{m+n} + \frac{\mathcal{C}^2}{6f^2}I^{\Delta K}_{m+n}, \tag{A21}$$

$$\Gamma^\mu_{m+n}(\Sigma^0) = \frac{\mathcal{C}^2}{3f^2}I^{\Delta K}_{m+n} - \frac{\mathcal{C}^2}{12f^2}I^{\Sigma^* K}_{m+n}, \tag{A22}$$

$$\Gamma^\mu_{m+n}(\Sigma^+) = -\frac{\mathcal{C}^2}{12f^2}I^{\Sigma^*\pi}_{m+n} + \frac{\mathcal{C}^2}{2f^2}I^{\Delta K}_{m+n} - \frac{\mathcal{C}^2}{6f^2}I^{\Xi^* K}_{m+n}, \tag{A23}$$

where the integral I^{TM}_{m+n} is written as,

$$\begin{aligned} I^{TM}_{m+n} = \bar{u}(p')\tilde{F}(q)\int\frac{\mathrm{d}^4k}{(2\pi)^4}\,\frac{\tilde{F}(k)^2}{D_M(k)}\Big\{&(k_\sigma + z\not{k}\gamma_\sigma)\frac{1}{\not{p}' - \not{k} - m_T}S^{\sigma\rho}(p'-k)\,(g_\rho{}^\mu + z\gamma_\rho\gamma^\mu) + \\ &(g^\mu{}_\sigma + z\gamma^\mu\gamma_\sigma)\frac{1}{\not{p} - \not{k} - m_T}S^{\sigma\rho}(p-k)\,(k_\rho + z\gamma_\rho\not{k})\Big\}u(p). \end{aligned} \tag{A24}$$

The contribution for the additional diagrams with intermediate decuplet states Fig. 1 o & p is expressed as

$$\Gamma^\mu_{o+p}(\Sigma^-) = \frac{\mathcal{C}^2}{12f^2}I^{\Sigma^*\pi}_{o+p} + \frac{\mathcal{C}^2}{6f^2}I^{\Delta K}_{o+p}, \tag{A25}$$

$$\Gamma^\mu_{o+p}(\Sigma^0) = \frac{\mathcal{C}^2}{3f^2}I^{\Delta K}_{o+p} - \frac{\mathcal{C}^2}{12f^2}I^{\Sigma^* K}_{o+p}, \tag{A26}$$

$$\Gamma^\mu_{o+p}(\Sigma^+) = -\frac{\mathcal{C}^2}{12f^2}I^{\Sigma^*\pi}_{o+p} + \frac{\mathcal{C}^2}{2f^2}I^{\Delta K}_{o+p} - \frac{\mathcal{C}^2}{6f^2}I^{\Xi^* K}_{o+p}, \tag{A27}$$

where the integral I_{o+p}^{TM} is written as

$$
\begin{aligned}
I_{o+p}^{TM} = \bar{u}(p')\tilde{F}(q) \int \frac{\mathrm{d}^4k}{(2\pi)^4} \frac{\tilde{F}(k)}{D_M(k)} \\
\Big\{ \frac{(-2k+q)^\mu}{-2kq+q^2} \Big(\tilde{F}(k-q) - \tilde{F}(k)\Big) (k_\sigma + z\not{k}\gamma_\sigma) \frac{1}{\not{p}' - \not{k} - m_T} S^{\sigma\rho}(p'-k) \left((k-q)_\rho + z\gamma_\rho(\not{k} - \not{q})\right) \\
+ \frac{(2k+q)^\mu}{2kq+q^2} \Big(\tilde{F}(k+q) - \tilde{F}(k)\Big) \left((k+q)_\sigma + z(\not{k}+\not{q})\gamma_\sigma\right) \frac{1}{\not{p} - \not{k} - m_T} S^{\sigma\rho}(p-k) \left(k_\rho + z\gamma_\rho \not{k}\right) \Big\} u(p).
\end{aligned}
\tag{A28}
$$

[1] A. Camsonne *et al.* (Jefferson Lab Hall A), JLab Measurement of the ^{4}He Charge Form Factor at Large Momentum Transfers, Phys. Rev. Lett. **112**, 132503 (2014), arXiv:1309.5297 [nucl-ex].

[2] A. M. Sirunyan *et al.* (CMS), Measurement of the triple-differential dijet cross section in proton-proton collisions at $\sqrt{s} = 8$ TeV and constraints on parton distribution functions, Eur. Phys. J. C **77**, 746 (2017), arXiv:1705.02628 [hep-ex].

[3] W. Xiong *et al.*, A small proton charge radius from an electron–proton scattering experiment, Nature **575**, 147 (2019).

[4] J. Bernauer *et al.* (A1), High-precision determination of the electric and magnetic form factors of the proton, Phys. Rev. Lett. **105**, 242001 (2010), arXiv:1007.5076 [nucl-ex].

[5] K. Kubodera, Y. Kohyama, K. Oikawa, *et al.*, Weak-interaction form factors of octet baryons in the cloudy bag model, Nucl. Phys. A **439**, 695 (1985).

[6] H. Dahiya, N. Sharma, P. K. Chatley, and G. Manmoha, Semi-leptonic octet baryon weak axial-vector form factors in the chiral constituent quark model, AIP Conf. Proc. **1149**, 361 (2009).

[7] J.-Y. Kim and H.-C. Kim, Electromagnetic form factors of singly heavy baryons in the self-consistent SU(3) chiral quark-soliton model, Phys. Rev. D **97**, 114009 (2018).

[8] T. Ito, W. Bentz, I. Cloët, A. Thomas, and K. Yazaki, The NJL-jet model for quark fragmentation functions, Phys. Rev. D **80**, 074008 (2009), arXiv:0906.5362 [nucl-th].

[9] T. Ohlsson and H. Snellman, Weak form factors for semileptonic octet baryon decays in the chiral quark model, Eur. Phys. J. C **6**, 285 (1999).

[10] Y. Yang, D.-Y. Chen, and Z. Lu, The electromagnetic form factors of Λ hyperon in the vector meson dominance model, Phys. Rev. D **100**, 10.1103/PhysRevD.100.073007 (2019), arXiv:1902.01242 [hep-ph].

[11] C. S. An and B. Saghai, Strangeness magnetic form factor of the proton in the extended chiral quark model, Phys. Rev. C **88**, 025206 (2013).

[12] R. N. Faustov and V. O. Galkin, Relativistic description of the Ξ_b baryon semileptonic decays, Phys. Rev. D **98**, 093006 (2018).

[13] T. Fuchs, J. Gegelia, and S. Scherer, Electromagnetic form factors of the nucleon in chiral perturbation theory, J. Phys. G **30**, 1407 (2004).

[14] B. Kubis and U.-G. Meissner, Low-energy analysis of the nucleon electromagnetic form factors, Nucl. Phys. A **679**, 698 (2001).

[15] P. Wang, D. B. Leinweber, A. W. Thomas, and R. D. Young, Chiral extrapolation of nucleon magnetic form factors, Phys. Rev. D **75**, 073012 (2007).

[16] P. Wang, D. B. Leinweber, A. W. Thomas, and R. D. Young, Strange magnetic form factor of the proton at $Q^2 = 0.23\mathrm{GeV}^2$, Phys. Rev. C **79**, 065202 (2009).

[17] P. Wang, D. B. Leinweber, A. W. Thomas, and R. D. Young, Chiral extrapolation of nucleon magnetic moments at next-to-leading-order, Phys. Rev. D **86**, 094038 (2012).

[18] J. M. M. Hall, D. B. Leinweber, and R. Young, Finite-volume and partial quenching effects in the magnetic polarizability of the neutron, Phys. Rev. D **89**, 054511 (2014).

[19] P. Wang, D. B. Leinweber, and A. W. Thomas, Strange magnetic form factor of the nucleon in a chiral effective model at next to leading order, Phys. Rev. D **89**, 033008 (2014).

[20] P. Wang, D. B. Leinweber, and A. W. Thomas, Pure sea-quark contributions to the magnetic form factors of Σ baryons, Phys. Rev. D **92**, 034508 (2015).

[21] H. Li, P. Wang, D. B. Leinweber, and A. W. Thomas, Spin of the proton in chiral effective field theory, Phys. Rev. C **93**, 045203 (2016).

[22] H. Li and P. Wang, Chiral extrapolation of nucleon axial charge ga in effective field theory, Chin. Phys. C **40**, 123106 (2016).

[23] C. R. Allton, W. Armour, D. B. Leinweber, A. W. Thomas, and R. D. Young, Chiral and continuum extrapolation of partially-quenched lattice results, Phys. Lett. B **628**, 125 (2005).

[24] P. Wang, D. Leinweber, A. Thomas, and R. Young, Chiral extrapolation of octet-baryon charge radii, Phys. Rev. D **79**, 094001 (2009), arXiv:0810.1021 [hep-ph].

[25] F. He and P. Wang, Nucleon electromagnetic form factors with a nonlocal chiral effective lagrangian, Phys. Rev. D **97**, 036007 (2018).

[26] F. He and P. Wang, Strange form factors of the nucleon with a nonlocal chiral effective lagrangian, Phys. Rev. D **98**, 036007 (2018).

[27] Y. Salamu, C.-R. Ji, W. Melnitchouk, A. W. Thomas, and P. Wang, Parton distributions from nonlocal chiral SU(3) effective theory: Splitting functions, Phys. Rev. D **99**, 014041 (2019).

[28] F. He and P. Wang, Sivers distribution functions of sea quark in proton with chiral Lagrangian, Phys. Rev. D **100**, 074032 (2019), arXiv:1904.06815 [hep-ph].

[29] F. He and P. Wang, Pauli form factors of electron and muon in nonlocal quantum electrodynamics, Eur. Phys. J. Plus **135**, 156 (2020), arXiv:1901.00271 [hep-ph].

[30] S. Boinepalli, D. Leinweber, A. Williams, J. Zanotti, and J. Zhang, Precision electromagnetic structure of octet baryons in the chiral regime, Phys. Rev. D **74**, 093005 (2006), arXiv:hep-lat/0604022.

[31] P. Shanahan, A. Thomas, R. Young, J. Zanotti, R. Horsley, Y. Nakamura, D. Pleiter, P. Rakow, G. Schierholz, and H. Stüben (CSSM, QCDSF/UKQCD), Magnetic form factors of the octet baryons from lattice QCD and chiral extrapolation, Phys. Rev. D **89**, 074511 (2014), arXiv:1401.5862 [hep-lat].

[32] P. Shanahan, A. Thomas, R. Young, J. Zanotti, R. Horsley, Y. Nakamura, D. Pleiter, P. Rakow, G. Schierholz, and H. Stüben, Electric form factors of the octet baryons from lattice QCD and chiral extrapolation, Phys. Rev. D **90**, 034502 (2014), arXiv:1403.1965 [hep-lat].

[33] E. E. Jenkins, Baryon masses in chiral perturbation theory, Nucl. Phys. B **368**, 190 (1992).

[34] E. E. Jenkins, M. E. Luke, A. V. Manohar, and M. J. Savage, Chiral perturbation theory analysis of the baryon magnetic moments, Phys. Lett. B **302**, 482 (1993), arXiv:hep-ph/9212226.

[35] P. Wang, Solid quantization for nonpoint particles, Can. J. Phys. **92**, 25 (2014).

[36] H. H. Patel, Package-X: A Mathematica package for the analytic calculation of one-loop integrals, Comput. Phys. Commun. **197**, 276 (2015).

[37] H.-W. Lin and K. Orginos, Strange Baryon Electromagnetic Form Factors and SU(3) Flavor Symmetry Breaking, Phys. Rev. D **79**, 074507 (2009), arXiv:0812.4456 [hep-lat].

[38] M. E. Carrillo-Serrano, W. Bentz, I. C. Cloët, and A. W. Thomas, Baryon Octet Electromagnetic Form Factors in a confining NJL model, Phys. Lett. B **759**, 178 (2016), arXiv:1603.02741 [nucl-th].

[39] X. Liu, K. Khosonthongkee, A. Limphirat, and Y. Yan, Study of baryon octet electromagnetic form factors in perturbative chiral quark model, J. Phys. G **41**, 055008 (2014), arXiv:1309.2063 [hep-ph].

[40] M. Tanabashi *et al.* (Particle Data Group), Review of Particle Physics, Phys. Rev. D **98**, 030001 (2018).

[41] V. Pascalutsa, M. Vanderhaeghen, and S. N. Yang, Electromagnetic excitation of the $\Delta(1232)$-resonance, Phys. Rept. **437**, 125 (2007), arXiv:hep/ph/0609004.

[42] L. M. Nath, B. Etemadi, and J. D. Kimel, Uniqueness of the interaction involving spin-32particles, Phys. Rev. D **3**, 2153 (1971).

[43] T. Janssens, R. Hofstadter, E. Hughes, and M. Yearian, Proton form factors from elastic electron-proton scattering, Phys. Rev. **142**, 922 (1966).

[44] C. Berger, V. Burkert, G. Knop, B. Langenbeck, and K. Rith, Electromagnetic form-factors of the proton at squared four momentum transfers between 10-fm**-2 and 50 fm**-2, Phys. Lett. B **35**, 87 (1971).

[45] L. Price, J. Dunning, M. Goitein, K. Hanson, T. Kirk, and R. Wilson, Backward-angle electron-proton elastic scattering and proton electromagnetic form-factors, Phys. Rev. D **4**, 45 (1971).

[46] H. Anklin *et al.*, Precision measurement of the neutron magnetic form-factor, Phys. Lett. B **336**, 313 (1994).

[47] R. Walker *et al.*, Measurements of the proton elastic form-factors for 1-GeV/c**2 <= Q**2 <= 3-GeV/C**2 at SLAC, Phys. Rev. D **49**, 5671 (1994).

[48] W. Bartel, F. Busser, W. Dix, R. Felst, D. Harms, H. Krehbiel, P. Kuhlmann, J. McElroy, J. Meyer, and G. Weber, Measurement of proton and neutron electromagnetic form-factors at squared four momentum transfers up to 3-GeV/c^2, Nucl. Phys. B **58**, 429 (1973).

[49] J. Golak, G. Ziemer, H. Kamada, H. Witala, and W. Gloeckle, Extraction of electromagnetic neutron form-factors through inclusive and exclusive polarized electron scattering on polarized He-3 target, Phys. Rev. C **63**, 034006 (2001), arXiv:nucl-th/0008008.

[50] P. Markowitz *et al.*, Measurement of the magnetic form factor of the neutron, Phys. Rev. C **48**, 5 (1993).

[51] E. Bruins *et al.*, Measurement of the neutron magnetic form-factor, Phys. Rev. Lett. **75**, 21 (1995).

[52] H. Anklin *et al.*, Precise measurements of the neutron magnetic form-factor, Phys. Lett. B **428**, 248 (1998).

[53] W. Xu *et al.*, The Transverse asymmetry A(T-prime) from quasielastic polarized He-3 (polarized e, e-prime) process and the neutron magnetic form-factor, Phys. Rev. Lett. **85**, 2900 (2000), arXiv:nucl-ex/0008003.

[54] G. Kubon *et al.*, Precise neutron magnetic form-factors, Phys. Lett. B **524**, 26 (2002), arXiv:nucl-ex/0107016.

[55] R. Madey *et al.* (E93-038), Measurements of G(E)n / G(M)n from the H-2(polarized-e,e-prime polarized-n) reaction to Q**2 = 1.45 (GeV/c)**2, Phys. Rev. Lett. **91**, 122002 (2003), arXiv:nucl-ex/0308007.

[56] W. Xu *et al.* (Jefferson Lab E95-001), PWIA extraction of the neutron magnetic form-factor from quasielastic polarized-He-3(polarized-e, e-prime) at Q**2 = 0.3-(GeV/c)**2 - 0.6-(GeV/c)**2, Phys. Rev. C **67**, 012201 (2003), arXiv:nucl-ex/0208007.

[57] K. Hanson, J. Dunning, M. Goitein, T. Kirk, L. Price, and R. Wilson, Large angle quasielastic electron-deuteron scattering, Phys. Rev. D **8**, 753 (1973).

[58] J. Murphy, Y. Shin, and D. Skopik, Proton form factor from 0.15 to 0.79 fm-2, Phys. Rev. C **9**, 2125 (1974), [Erratum: Phys.Rev.C 10, 2111–2111 (1974)].

[59] G. Hohler, E. Pietarinen, I. Sabba Stefanescu, F. Borkowski, G. Simon, V. Walther, and R. Wendling, Analysis of Electromagnetic Nucleon Form-Factors, Nucl. Phys. B **114**, 505 (1976).

[60] G. Simon, C. Schmitt, F. Borkowski, and V. Walther, Absolute electron Proton Cross-Sections at Low Momentum Transfer Measured with a High Pressure Gas Target System, Nucl. Phys. A **333**, 381 (1980).

[61] T. Eden *et al.*, Electric form factor of the neutron from the $^2H(\vec{e},e'\vec{n})^1H$ reaction at $Q^2 = 0.255$ (GeV/c)^2, Phys. Rev. C **50**, 1749 (1994).

[62] C. Herberg *et al.*, Determination of the neutron electric form-factor in the D(e,e' n)p reaction and the influence of nuclear binding, Eur. Phys. J. A **5**, 131 (1999).

[63] M. Ostrick *et al.*, Measurement of the neutron electric form-factor G(E,n) in the quasifree H-2(e(pol.),e' n(pol.))p reaction, Phys. Rev. Lett. **83**, 276 (1999).

[64] I. Passchier *et al.*, The Charge form-factor of the neutron from the reaction polarized H-2(polarized e, e-prime n) p, Phys. Rev. Lett. **82**, 4988 (1999), arXiv:nucl-ex/9907012.

[65] J. Bermuth *et al.*, The Neutron charge form-factor and target analyzing powers from polarized-He-3 (polarized-e,e-prime n) scattering, Phys. Lett. B **564**, 199 (2003), arXiv:nucl-ex/0303015.

[66] G. Warren *et al.* (Jefferson Lab E93-026), Measurement of the electric form-factor of the neutron at $Q^2 = 0.5$ and 1.0 GeV^2/c^2, Phys. Rev. Lett. **92**, 042301 (2004), arXiv:nucl-ex/0308021.

[67] D. Glazier *et al.*, Measurement of the electric form-factor of the neutron at Q**2 = 0.3-(GeV/c)**2 to 0.8-(GeV/c)**2, Eur. Phys. J. A **24**, 101 (2005), arXiv:nucl-ex/0410026.